Rapid Communications

Chiral quasiparticle tunneling between quantum Hall edges in proximity with a superconductor

M. T. Wei,[1] A. W. Draelos,[1] A. Seredinski,[1] C. T. Ke,[1] H. Li,[2] Y. Mehta,[2] K. Watanabe,[3] T. Taniguchi,[3] M. Yamamoto,[4] S. Tarucha,[4] G. Finkelstein,[1] F. Amet,[2] and I. V. Borzenets[5,*]

[1]*Department of Physics, Duke University, Durham, North Carolina 27708, USA*
[2]*Department of Physics and Astronomy, Appalachian State University, Boone, North Carolina 28607, USA*
[3]*Advanced Materials Laboratory, NIMS, Tsukuba 305-0044, Japan*
[4]*Center for Emergent Matter Science (CEMS), RIKEN, Wako-shi, Saitama 351-0198, Japan*
[5]*Department of Physics, City University of Hong Kong, Kowloon, Hong Kong SAR*

(Received 4 May 2019; revised manuscript received 21 July 2019; published 10 September 2019)

We study a two-terminal graphene Josephson junction with contacts shaped to form a narrow constriction, less than 100 nm in length. The contacts are made from type-II superconducting contacts and able to withstand magnetic fields high enough to reach the quantum Hall regime in graphene. In this regime, the device conductance is determined by edge states, plus the contribution from the constricted region. In particular, the constriction area can support supercurrents up to fields of ∼2.5 T. Additionally, enhanced conductance is observed through a wide range of magnetic fields and gate voltages. This additional conductance and the appearance of supercurrent is attributed to the tunneling between counterpropagating quantum Hall edge states along opposite superconducting contacts.

DOI: 10.1103/PhysRevB.100.121403

In the past few years, there has been a renewed interest in quantum Hall (QH) states supported along superconducting (SC) materials. Experimentally, this was prompted by several groups successfully making high-transparency type-II superconducting contacts to both encapsulated graphene and III-V semiconductor heterostructures [1–10]. Meanwhile, theoretical works have predicted multiple exciting phenomena in structures combining the quantum Hall effect and superconductivity [11–30]. In particular, it is expected that Andreev edge states (AES)—hybrid modes involving a linear superposition of electron and hole states—should be formed at these QH-SC interfaces [9,14–17]. Experimental observation of the interference of such states has been recently reported [31]. Furthermore, these structures have been predicted to support Majorana zero modes and parafermions when the symmetry-breaking QH edge states are coupled to SC [19–22]. Here, we explore AES and tunneling between two superconducting contacts across a narrow region of graphene in the quantum Hall regime.

Our device design is shown in Fig. 1. A graphene crystal of 1 μm × 1 μm is contacted on two sides by the superconductor molybdenum rhenium (MoRe). The contacts are asymmetric, with one interface being flat, and the other having a "T" shape. The 350-nm-wide leg of the T extends into the graphene, such that the shortest separation between contacts is $l \sim 90$ nm. The graphene device is assembled by a standard stamping technique [32], where monolayer graphene is sandwiched by hexagonal boron nitride (hBN) and placed onto a graphite back gate [Fig. 1(b)]. The back gate-graphene distance is ∼40 nm (confirmed by atomic force microscopy), and metal leads of Cr/Au (5 nm/110 nm) are used to make contact with the back gate. Carefully calibrated etching of the stack allows us to avoid shorting to the graphite back gate.

The sample was measured with a pseudo-four-probe setup in a Leiden Cryogenics dilution refrigerator with a base electron temperature of ∼50 mK (at zero field) to ∼60 mK (at high fields). A dc bias current along with a small ac excitation is supplied by a combination of an NI USB-6363 digital acquisition device and a lock-in amplifier. The measured voltage is initially amplified by a home-made, low-frequency, low-noise amplifier. Three-stage *RC* filtering, a stainless steel powder filter, and resistive lines were all employed to lower the high-frequency noise that can suppress the supercurrent. Carrier density in the graphene was tuned via a back gate voltage applied to the graphite layer, where the gate capacitance is $C_G \approx 70$ nF/cm^2. Magnetic fields are applied perpendicular to the plane of the graphene sheet.

The differential resistance $R = dV/dI$ is shown in Fig. 1(c) as a function of the dc bias current I_{dc} and back gate voltage V_G, taken at magnetic field $B = 2$ T (sufficient to place the device firmly in the QH regime for $V_G < 1.5$ V as seen in Fig. 3). Near zero bias, areas of suppressed resistance can be clearly observed, indicating the presence of supercurrent [Fig. 1(d)]. Pockets of supercurrent are seen at multiple locations in V_G. The majority of superconducting pockets are found at areas corresponding to transitions between two QH plateaus, consistent with previous works [4–6]. (It appears that regions where the filling factor is not well defined lead to favorable conditions in forming an Andreev bound state.) However, smaller pockets exist on top of conductance plateaus as well, notably at $V_G \approx 0.44$ V in Fig. 1(c). Outside of the superconducting pockets, at zero bias one can observe an enhanced resistance, as shown in Fig. 1(e). This is associated with conduction via tunneling, revealing the presence of a superconducting gap. Note that for $B = 2$ T and $V_G > 1.5$ V

*iborzene@cityu.edu.hk

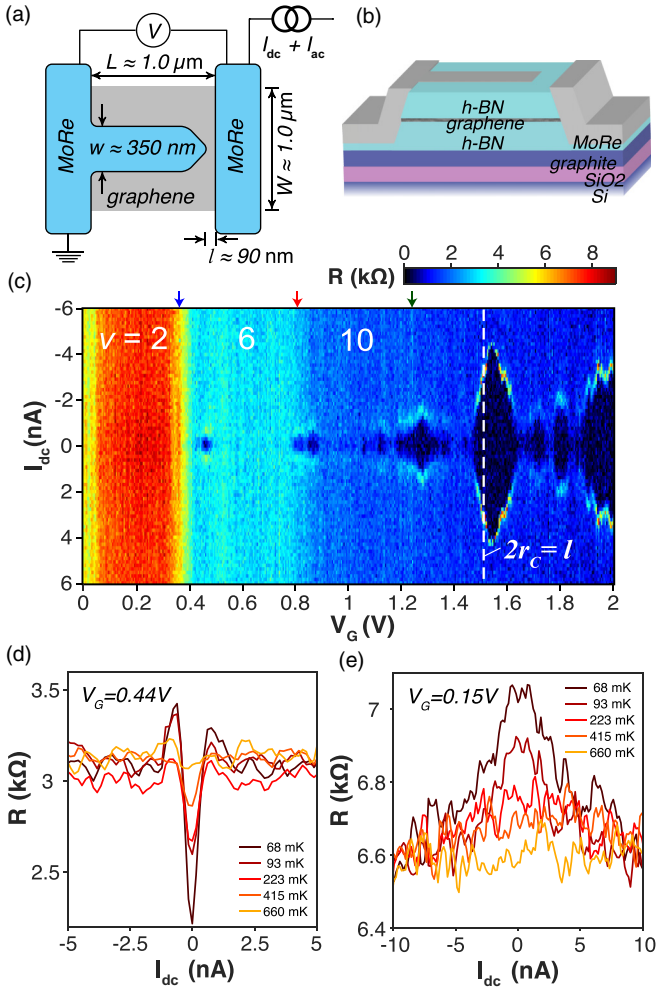

FIG. 1. (a) Schematic of the graphene Josephson junction with asymmetric contacts, measured with a four-probe current-biased setup. The finger of the T-shaped contact is separated from the opposing contact by about 90 nm. (b) Three-dimensional (3D) representation of the T-shaped junction illustrating the graphene-hBN stack with the graphite back gate. (c) Differential resistance $R = dV/dI$ vs dc bias current I_{dc} and gate voltage V_G taken at a perpendicular magnetic field of $B = 2$ T. Pockets of suppressed resistance (superconductivity) are observed at several gate voltages through the region including on the quantum Hall plateaus, at the transition between two filling factors, and in the semiclassical region. The arrows at the top edge denote transitions between the different filling factors ν, while the white, dashed line denotes V_G at which the cyclotron radius becomes equal to half the constriction width l (the onset of the semiclassical region). (d), (e) Resistance vs I_{dc} for selected gate values. (d) shows enhanced zero-bias resistance, a signature of the superconducting gap. (e) demonstrates the observance of supercurrent.

the cyclotron radius satisfying $2r_c > 90$ nm places the sample in the semiclassical regime at the constriction [1].

Figure 2(a) shows this same differential resistance versus δB and V_G at zero bias, as the magnetic field is varied only slightly to investigate the periodicity of the observed supercurrent [4,5,18]. [Figure 2(a) presents data at $B = 2.5$ T, the highest measured field where supercurrent was still observed.] Low resistances at $I_{dc} = 0$ again show the supercurrent, which

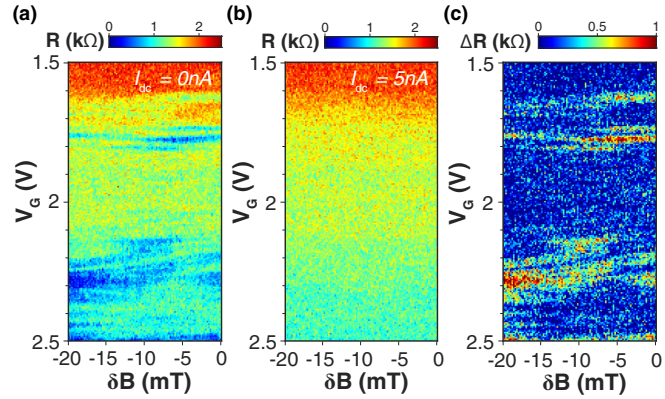

FIG. 2. The dependence of differential resistance R on magnetic field: $B = 2.5$ T $+ \delta B$ as a function of gate voltages V_G and bias current. (a) Resistance dips at $I_{dc} = 0$ nA indicate pockets of supercurrent. (b) Superconducting signatures are fully suppressed at $I_{dc} = 5$ nA. (c) The resistance difference ΔR between $I_{dc} = 5$ and 0 nA. No periodic oscillations of supercurrent in field are observed. This suggests that the supercurrent is not mediated by the QH states along the graphene edges, as a superconducting quantum interference device (SQUID)-like pattern would be expected to emerge.

is contrasted by Fig. 2(b) taken at a dc bias of $I_{dc} = 5$ nA. Such I_{dc} is sufficient to suppress all superconducting features, while preserving plateau quantization. The suppression of resistance can be quantified by subtracting the zero-bias resistance from the high-bias resistance $\Delta R = R_{5\,\mathrm{nA}} - R_{0\,\mathrm{nA}}$, shown in Fig. 2(c), where high ΔR indicate regions of supercurrent [5]. Note that previous works showed a full suppression of supercurrent for devices of length longer than 1 μm, suggesting that the observed supercurrent is mediated by the constriction [5].

Indeed, unlike previous works, these pockets of supercurrent do not show periodic oscillations with magnetic field [4,5]. For a Josephson junction of area $A \approx 0.7\ \mu\mathrm{m}^2$ with supercurrent supported along the circumference, oscillations with a period of $\Delta B \approx 0.5$ mT are expected [4,5,33]. Instead, the observed features evolve slowly and aperiodically on the scale of $\Delta B \sim 10$ mT, suggesting that the supercurrent does not flow along the graphene-vacuum edges. Previous works showed (but did not discuss) that the observed supercurrent envelope evolved on a similar scale [4,5]. Recent work accessing the AES states directly has showed that a single trapped vortex in the superconductor can dramatically alter the phase of the AES [31]. Moreover, the measured normal resistance (resistance at I_{dc} large enough to suppress all superconducting features) of the QH plateaus is lower than the expected quantized fractions of $h/2e^2$. This strongly suggests the existence of additional conducting channels beyond the standard QH edge states.

We next measure the sample conductance using only a dc bias of $I_{dc} = 5$ nA (suppressing the features associated with superconductivity) without any ac excitation in order to avoid measurement errors due to stray capacitance. Figure 3(a) shows the fan diagram of conductance versus back gate voltage and magnetic field up to 7 T. Above 4 T, we see the $\nu = 1$ plateau developing in addition to the $\nu = 2, 6, 10$

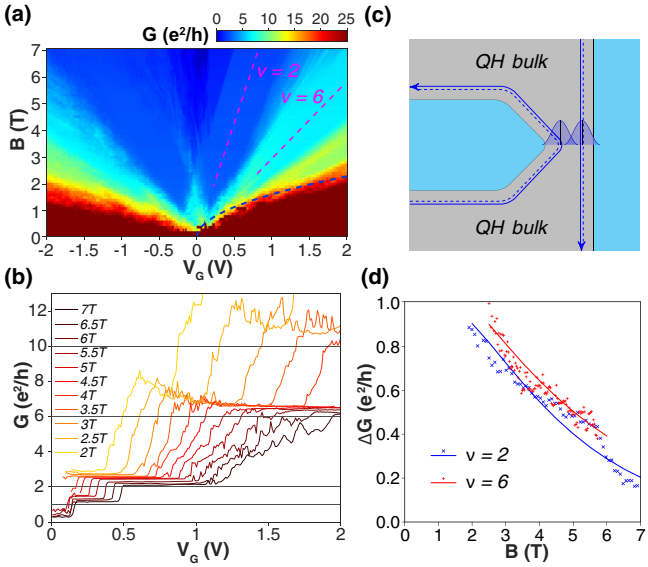

FIG. 3. Field-dependent conductance. (a) The fan diagram of measured conductance from 0 to 7 T. The blue dashed line represents the boundary at which the cyclotron radius is half the constriction length $r = 45$ nm. The magenta dashed lines follow the centers of the $\nu = 2, 6$ plateaus. (b) The measured conductance as a function of back gate voltages V_G taken at several magnetic fields from 2 to 7 T. (c) Schematic of the QH edge states at the constriction. Each edge state is statistically distributed around a central location (blue lines). At the constriction, a significant overlap in the distributions of the opposing edge states is expected, mediating tunneling. (d) Enhancement in the measured conductance ΔG for the marked line cuts in (a) at $\nu = 2, 6$ along the center of the QH plateaus. The dots are the measured data, while the solid lines are fitted conductances simulating the contribution due to tunneling via overlapping QH states running along the graphene-superconductor interface.

plateaus previously studied. Figure 3(b) shows selected cross sections of the conductance as a function of back gate voltage at magnetic fields from 2 to 7 T, compared to the expected value of each plateau (horizontal black lines). It is apparent that the height of each plateau decays monotonically with increasing magnetic field, though without fully reaching the expected value of QH conductance. Note that this decreasing conductance with increasing field cannot be attributed to the growing finite resistance of the superconductor near its critical field (as in the case of niobium in Ref. [34]) because MoRe alloys do not exhibit a finite resistance for the magnetic fields used here [2].

The existence of nonperiodic supercurrents at 2.5 T and field-dependent conductance can both be attributed to the coupling of QH edge states across the short 90-nm channel. For lower magnetic fields, when the cyclotron radius $r = \hbar\sqrt{n\pi}/eB > l/2 \approx 45$ nm [blue dashed line in Fig. 3(a)], the short channel is in the semiclassical regime [1]. (Here, n is the carrier density.) As such, supercurrent can be supported by conventional Andreev bound states. When $r \ll 45$ nm, the supercurrents could be mediated via quantum mechanical tunneling between QH edge modes [35–39]. In the normal conduction regime, the enhanced conductance ΔG approaching $\nu e^2/h$ suggests that the overall conductance can be written as

$$G_{\text{total}} = G_{\text{QH}} + G_{\text{tunneling}},$$

where G_{QH} is the expected quantized QH conductance of the edge channels along the vacuum edges and $G_{\text{tunneling}} = \Delta G$ is the additional conductance from the T-shaped short channel.

Demonstrated schematically in Fig. 3(c), the lines represent the centers of the counterpropagating edge states. The overlap between these wave functions propagating along each contact in the short channel is what mediates the supercurrent by tunneling. Note that such scheme of conduction is similar to tunneling *across* a point contact constriction in the quantum Hall regime [35–39]. Here, however, the constriction is defined by the superconductors which simultaneously act as the source and drain electrodes. The constriction is tuned by the back gate instead of the point contact split gates.

The measured enhanced conductance ΔG taken along the red dashed lines shown in Fig. 3(a) for $\nu = 2$ and $\nu = 6$ is plotted in Fig. 3(d) as dots. [The red dashed lines in Fig. 3(a) represent the center of the quantized plateau.] The solid lines of Fig. 3(d) are a fit of the data to

$$\Delta G = A \int_{-\infty}^{\infty} \exp\frac{-(x - X_0)^2}{2W_0^2} \exp\frac{-(x - l + X_0)^2}{2W_0^2} dx.$$

Here, we take the collective opposing edge states to have Gaussian distributions that are centered at a distance X_0 from the graphene-superconductor edge, and have a width of $W_0 = l_B$ [40] (where $l_B \approx 26\,\text{nm}/\sqrt{B}$ is the magnetic wavelength). The two edges themselves are separated by a length $l = 90$ nm. The enhanced normal conduction ΔG is then proportional to the amount of overlap between the two distributions with a proportionality factor A. We use $A \approx 0.72$ (for $\nu = 2$) and 0.77 (for $\nu = 6$), and $X_0 \approx 33$ nm as the fitting parameters.

Thus, the above fit represents a situation where the collective edge states become narrower with increasing magnetic field, but remain separated by a constant distance. For an individual, regular QH edge state, however, one expects X_0 to scale with magnetic field as $X_0 = k_x l_B^2 \propto 1/B$ [40]. Including a field dependence into the variable X_0 does not produce a desirable fit. Unlike for the case of graphene-vacuum edges, the filling factor at the graphene-superconductor interface may not be well defined as the presence of the MoRe contacts locally n-dopes the graphene. This effect becomes more pronounced at the constriction where the contact doping may screen the back gate. The shape of the constriction itself may play a role in the amount of overlap (and the population of) the opposing edge states. Thus it is difficult to quantitatively determine the exact wave functions at play in the constriction. Nevertheless, the strong but aperiodic supercurrent as well as enhanced conduction in the normal regime (supported by our fitting scheme) leads us to conclude that we observe a supercurrent that is mediated via tunneling between the two edge states at the constriction.

In our device, we expect the conductance of the QH edge states to reach their theoretically expected values by $B \approx 10$ T. Knowing both the amount of overlap and the strength of interactions between two QH edge states is important when coupling them to produce topological states such as

parafermions [22]. This experiment provides an important step towards the design of QH-SC structures that are capable of supporting such non-Abelian excitations.

In conclusion, a short channel in a Josephson junction with T-shaped asymmetric contacts has been shown to mediate a nonperiodic supercurrent and cause a nontrivial extra conductance that gradually decays at higher fields. This result is tunneling evidence of the chiral electron-hole hybrid modes between two superconductors. Theoretical studies on this type of chiral quasiparticle tunneling are still needed. We anticipate that further investigation on this tunneling conductance could help us understand the characteristics of chiral electron-hole hybrid states and ultimately pursue topological superconductivity in QH/SC graphene devices.

Low-temperature electronic measurements performed by M.T.W., A.W.D., and G.F. were supported by ARO Award No. W911NF16-1-0122 and NSF Awards No. ECCS-1610213 and No. DMR-1743907. Lithographic fabrication and characterization of the samples performed by M.T.W. and A.S. were supported by the Division of Materials Sciences and Engineering, Office of Basic Energy Sciences, U.S. Department of Energy, under Award No. DE-SC0002765. S.T. and M.Y. acknowledges KAKENHI (Grants No. 38000131 and No. 17H01138). I.V.B. acknowledges CityU New Research Initiatives/Infrastructure Support from Central (APRC) No. 9610395, and the Hong Kong Research Grants Council (ECS) Project No. 9048125. We thank A. Chang, H. Baranger, and G. Zhang for fruitful discussions about the data.

[1] M. Ben Shalom, M. J. Zhu, V. I. Fal'ko, A. Mishchenko, A. V. Kretinin, K. S. Novoselov, C. R. Woods, K. Watanabe, T. Taniguchi, A. K. Geim, and J. R. Prance, Nat. Phys. **12**, 318 (2016).

[2] V. E. Calado, S. Goswami, G. Nanda, M. Diez, A. R. Akhmerov, K. Watanabe, T. Taniguchi, T. M. Klapwijk, and L. M. K. Vandersypen, Nat. Nanotechnol. **10**, 761 (2015).

[3] Z. Wan, A. Kazakov, M. J. Manfra, L. N. Pfeiffer, K. W. West, and L. P. Rokhinson, Nat. Commun. **6**, 7426 (2015).

[4] F. Amet, C. T. Ke, I. V. Borzenets, J. Wang, K. Watanabe, T. Taniguchi, R. S. Deacon, M. Yamamoto, Y. Bomze, S. Tarucha, and G. Finkelstein, Science **352**, 966 (2016).

[5] A. W. Draelos, M. T. Wei, A. Seredinski, C. T. Ke, Y. Mehta, R. Chamberlain, K. Watanabe, T. Taniguchi, M. Yamamoto, S. Tarucha, I. V. Borzenets, F. Amet, and G. Finkelstein, J. Low Temp. Phys. **191**, 288 (2018).

[6] A. Seredinski, A. Draelos, M.-T. Wei, C.-T. Ke, T. Fleming, Y. Mehta, E. Mancil, H. Li, T. Taniguchi, K. Watanabe, S. Tarucha, M. Yamamoto, I. V. Borzenets, F. Amet, and G. Finkelstein, MRS Adv. **3**, 2855 (2018).

[7] A. Seredinski, A. W. Draelos, E. G. Arnault, M.-T. Wei, H. Li, K. Watanabe, T. Taniguchi, F. Amet, and G. Finkelstein, arXiv:1901.05928.

[8] G.-H. Lee, K.-F. Huang, D. K. Efetov, D. S. Wei, S. Hart, T. Taniguchi, K. Watanabe, A. Yacoby, and P. Kim, Nat. Phys. **13**, 693 (2017).

[9] G.-H. Park, M. Kim, K. Watanabe, T. Taniguchi, and H.-J. Lee, Sci. Rep. **7**, 10953 (2017).

[10] M. R. Sahu, X. Liu, A. K. Paul, S. Das, P. Raychaudhuri, J. K. Jain, and A. Das, Phys. Rev. Lett. **121**, 086809 (2018).

[11] M. Ma and A. Y. Zyuzin, Europhys. Lett. **21**, 941 (1993).

[12] A. Y. Zyuzin, Phys. Rev. B **50**, 323 (1994).

[13] M. P. A. Fisher, Phys. Rev. B **49**, 14550 (1994).

[14] Y. Takagaki, Phys. Rev. B **57**, 4009 (1998).

[15] H. Hoppe, U. Zülicke, and G. Schön, Phys. Rev. Lett. **84**, 1804 (2000).

[16] N. M. Chtchelkatchev and I. S. Burmistrov, Phys. Rev. B **75**, 214510 (2007).

[17] I. M. Khaymovich, N. M. Chtchelkatchev, I. A. Shereshevskii, and A. S. Mel'nikov, Europhys. Lett. **91**, 17005 (2010).

[18] J. A. M. van Ostaay, A. R. Akhmerov, and C. W. J. Beenakker, Phys. Rev. B **83**, 195441 (2011).

[19] D. J. Clarke, J. Alicea, and K. Shtengel, Nat. Commun. **4**, 1348 (2013).

[20] R. S. K. Mong, D. J. Clarke, J. Alicea, N. H. Lindner, P. Fendley, C. Nayak, Y. Oreg, A. Stern, E. Berg, K. Shtengel, and M. P. A. Fisher, Phys. Rev. X **4**, 011036 (2014).

[21] D. J. Clarke, J. Alicea, and K. Shtengel, Nat. Phys. **10**, 877 (2014).

[22] J. Alicea and P. Fendley, Annu. Rev. Condens. Matter Phys. **7**, 119 (2016).

[23] P. San-Jose, J. L. Lado, R. Aguado, F. Guinea, and J. Fernández-Rossier, Phys. Rev. X **5**, 041042 (2015).

[24] B. Zocher and B. Rosenow, Phys. Rev. B **93**, 214504 (2016).

[25] L. Cohnitz, A. De Martino, W. Häusler, and R. Egger, Phys. Rev. B **96**, 140506(R) (2017).

[26] Y. Alavirad, D. Clarke, A. Nag, and J. D. Sau, Phys. Rev. Lett. **119**, 217701 (2017).

[27] O. Gamayun, J. A. Hutasoit, and V. V. Cheianov, Phys. Rev. B **96**, 241104(R) (2017).

[28] X.-L. Huang and Y. V. Nazarov, Phys. Rev. Lett. **118**, 177001 (2017).

[29] F. Finocchiaro, F. Guinea, and P. San-Jose, Phys. Rev. Lett. **120**, 116801 (2018).

[30] C. Repellin, A. M. Cook, T. Neupert, and N. Regnault, npj Quantum Mater. **3**, 14 (2018).

[31] L. Zhao, E. G. Arnault, A. Bondarev, A. Seredinski, T. Larson, A. W. Draelos, H. Li, K. Watanabe, T. Taniguchi, F. Amet, H. U. Baranger, and G. Finkelstein, arXiv:1907.01722.

[32] C. R. Dean, A. F. Young, I. Meric, C. Lee, L. Wang, S. Sorgenfrei, K. Watanabe, T. Taniguchi, P. Kim, K. L. Shepard, and J. Hone, Nat. Nanotechnol. **5**, 722 (2010).

[33] M. Tinkham, *Introduction To Superconductivity* (McGraw-Hill, New York, 1996).

[34] P. Rickhaus, M. Weiss, L. Marot, and C. Schönenberger, Nano Lett. **12**, 1942 (2012).

[35] K. Moon, H. Yi, C. L. Kane, S. M. Girvin, and M. P. A. Fisher, Phys. Rev. Lett. **71**, 4381 (1993).

[36] E.-A. Kim and E. Fradkin, Phys. Rev. B **67**, 045317 (2003).

[37] S. Roddaro, V. Pellegrini, F. Beltram, G. Biasiol, L. Sorba, R. Raimondi, and G. Vignale, Phys. Rev. Lett. **90**, 046805 (2003).

[38] I. P. Radu, J. B. Miller, C. M. Marcus, M. A. Kastner, L. N. Pfeiffer, and K. W. West, Science **320**, 899 (2008); X. Lin, C. Dillard, M. A. Kastner, L. N. Pfeiffer, and K. W. West, Phys. Rev. B **85**, 165321 (2012).

[39] F. Martins, S. Faniel, B. Rosenow, H. Sellier, S. Huant, M. G. Pala, L. Desplanque, X. Wallart, V. Bayot, and B. Hackens, Sci. Rep. **3**, 1416 (2013).

[40] Y. Zheng and T. Ando, Phys. Rev. B **65**, 245420 (2002).